

CHAPTER 178

Fundamental Characteristics of Wave Transformation Around Artificial Reefs

Toshio Aono¹

Eric C. Cruz²

Abstract

The fundamental characteristics of the wave field around an existing artificial reef in Japan are studied based on field measurements and wave simulations using a nonlinear wave model that takes reef porosity into account. Results of two-dimensional simulations and comparison with field data of significant wave heights and reef velocities indicate characteristic wave evolution of nonbreaking and breaking waves and confirm the damping effect of the reef.

1. INTRODUCTION

Artificial reefs are a type of submerged breakwater. Unlike ordinary submerged breakwaters, however, they are usually designed with a permeable interior, a broad crown and steep face slopes. A permeable interior allows better water exchange with the sea when incident waves are small and yet induces wave energy dissipation through porous damping when the incident waves are high. A broad crown improves the damping effect of the reef over a wider frequency range while the steep face slopes are structural merits exploited when certain types of armor units are used to protect the reef when used as a breakwater. Hence, there are at least three important properties which must be considered when analyzing an actual artificial reef: (1) porosity (2) a wide depth regime, that is, shallow on the reef crown and deep on either side; and (3) steep face slopes.

A considerable number of artificial reefs have been constructed near the coasts in Japan, but there are no published reports on detailed field measurements around such structures. Part of this paper reports on a series of field measurements around Yugawara artificial reef which is one of such existing reefs in a Japanese coast. These measurements include the water surface profiles as well as reef velocities on

¹ Senior Research Engineer, Numerical Analysis Laboratory, Technical Research Institute, Toa Corporation, 1-3 Anzen-cho Tsurumi-ku Yokohama 230, Japan.

² Research Engineer, ditto

the reef crown.

Results obtained from a synthesis from these field measurements were used to verify the applicability of a mathematical model originally developed for wave transformation on porous beds. Mathematical models have been proposed in recent years to model the wave field around submerged structures. Inclusion of wave non-linearity in these models is important due to the small depth on the crowns of submerged structures. A second requisite is good dispersivity in order to reproduce frequency-dependent phenomena such as propagation in deep water, transformation and wave grouping of irregular waves and wave decomposition at the lee. For an artificial reef used as a submerged breakwater, the porous interior dissipates wave energy and hence porosity is an important property that affects the evolution of the wave.

This paper is part of a study which aims to analyze the effects of the existing Yugawara reef with a broadened crown on the surrounding coastal environment, particularly on the revetment which protects the adjacent coast. As an initial step, a simplified treatment of the wave field is chosen to serve as basis for launching a more detailed set of computations. The objective of the present paper is therefore to identify basic characteristics of the wave field based on field measurements and wave simulations with practical assumptions on reef composition and wave dimensionality.

2. FIELD MEASUREMENTS

General Description of Yugawara Artificial Reef

The layout of the existing reef is shown in **Fig. 1(a)** and the section through the center is shown in **Fig. 1(b)**. The reef was constructed to reduce the damage during high wave conditions to the vertical wave-absorbing revetment onshore which, in turn, protects the structures on the coast used for commercial fishing. The reef crown is 170m long and 70m wide. The crown width was increased from the previous 32m (shown dashed in **Fig. 1**) to make it more effective in dissipating the wave energy over a wider range of relative

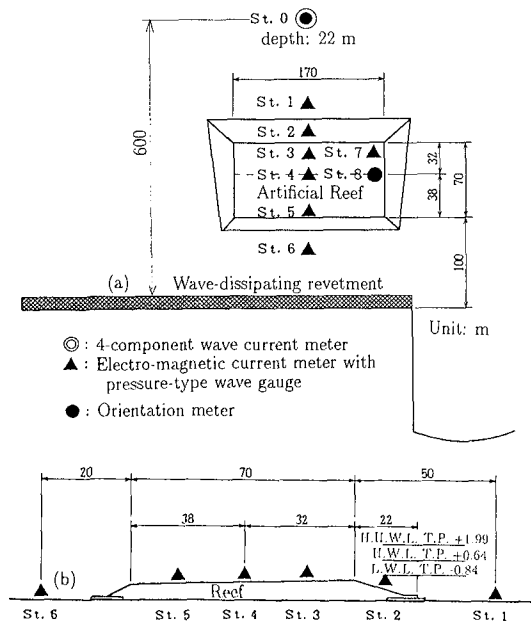


Fig.1 Layout of Yugawara artificial reef and measuring devices. (a)plan view (b)cross section

water depths. The seaward slope is 1:3 while the shoreward slope is 1:2. The seaward slope and the seaward 32m of the crown are protected with 10-ton X-block armor units while the shoreward slope and the remaining portion of the crown are covered with 2-ton armor stones. The reef interior consists of 30 to 200kg medium-sized stones. The crown is submerged about 1.5m from mean water level and the depth to the seabed is around 8.5m at the crown center.

Field Measurements

Field measurements were conducted continuously for 2 months from February 1 to March 31, 1994. The measuring devices and their location are shown in Fig. 1. The water depths and surface elevations were measured by pressure-type gauges and velocity components at a fixed distance from the reef bed were measured directly using electro-magnetic current meters. Incident wave conditions were based on measurements at station 0 located 600 m from the revetment at a depth of 22 m. Six stations were disposed along the reef centerline with Stations 3, 4 and 5 on the shallow crown while Stations 7 and 8 were installed as shown to evaluate the effect of reef edge. The bed configuration and reef shape were determined from design drawings. However, field measurements of depths indicate that the bed slope has changed from its design value of 1:30 to 1:39 and the seaward slope from its design value of 1:3 to 1:3.16 due probably to slump of the reef and scouring at the toe. These measured slopes were applied to the bathymetry used in the computations .

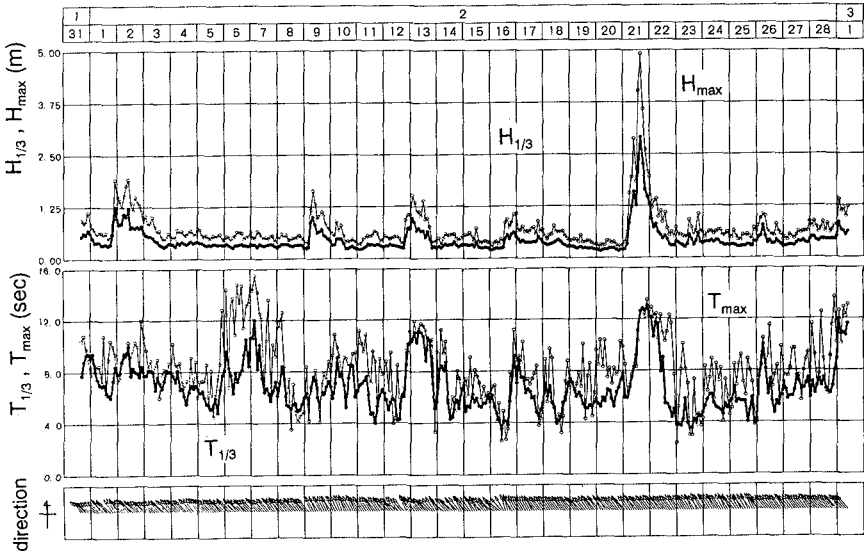


Fig. 2 Time series of $H_{1/3}$, $T_{1/3}$, H_{max} , T_{max} and incident wave direction

Fig. 2 shows the observed time series of the significant wave height and period, maximum wave height and period and incident wave direction. The critical wave occurred on February 21 with a significant wave height of 2.90m and maximum

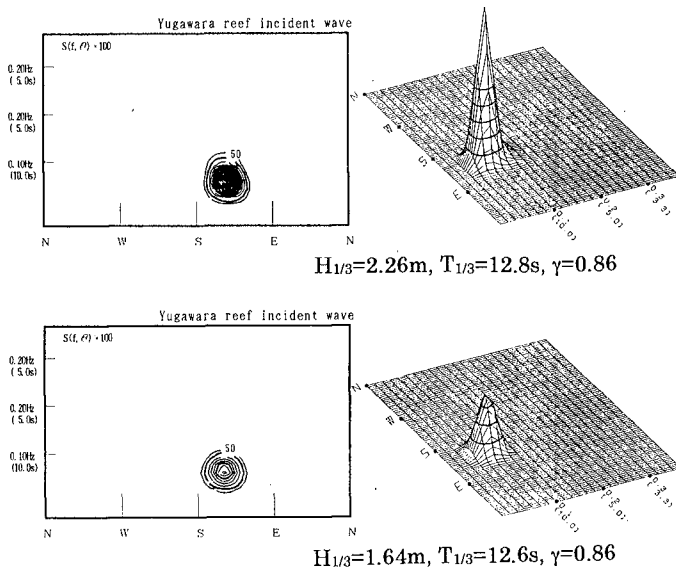


Fig.3 Directional spectrum (incident wave)

wave height of 5m. This wave was due to a low-pressure atmosphere. The significant wave period fluctuates but the highest value coincided with the significant wave height. This critical wave condition was used in the simulation. Incident wave direction was almost constant during the entire observation period. The wave direction was oriented almost normally to the reef. **Fig.3** shows the directional spectrum of incident wave. The method of calculation is EMEP by Hashimoto(1992). The shape of this directional spectrum is a single peak type and the long crestedness parameter is 0.86 so the directional spreading is relatively small. Observed directional spectrum data show an almost similar tendency.

Fig.4 shows the significant wave heights $H_{1/3}$ at stations along the center of the reef. We observed that it first increases on approaching the reef's seaward slope. Then it decreases abruptly due to breaking. Along the reef crown, the significant height continues to decrease due to the damping action of the porous interior. However, the rate of decrease is smaller than that due to

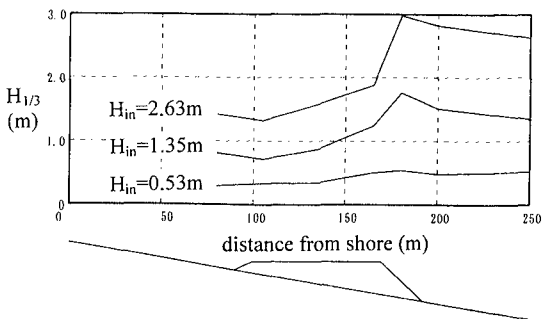


Fig.4 Distribution of $H_{1/3}$ along the center of reef

breaking. At the back of the reef, the wave height can still increase depending on the incident wave conditions.

3. MODEL EQUATIONS FORMULATION AND ANALYSIS

Model Equations

The basic depth-averaged nonlinear equations for horizontal one-dimensional wave transformation over porous beds have been derived using the perturbation method (Isobe et al., 1991; Cruz, et al., 1992). The leading order of nonlinearity has been included but nondispersive waves were vicariously assumed. The model can reproduce the generation of higher harmonics on the shallow crown but cannot predict the decomposition of waves beyond the structure. By reformulating the basic governing equations in the water and porous layers as a potential flow problem in terms of nondimensionalized variables, Cruz et al. (1996) obtained a set of Boussinesq equations for porous beds. These equations possess a second-order accurate linear dispersion relation and are applicable to weakly dispersive waves. By extending the linear dispersion relation to fourth-order accuracy through the addition of higher-order momentum terms, the Extended Boussinesq Equations for Porous Beds were obtained. For two-dimensional wave transformation, they are written as:

$$\eta_x + [(h + \eta)u]_x + (\varepsilon h_s u_s)_x = 0 \quad (1)$$

$$u_t + \frac{1}{2}(u_s^2)_x + g\eta_x - \varphi + F_\varepsilon + F_B = O(\delta\mu^2, \mu^4) \quad (2)$$

$$C_r \left[u_{st} + \frac{1}{2}(u_s^2)_x \right] + g\eta_x + \alpha u_s - \varphi_s = O(\delta\mu^2, \mu^4) \quad (3)$$

where η is the water surface displacement, u and u_s the depth-averaged velocities in the water and porous layers, ε the porosity, g the gravity acceleration, h and h_s the thickness of the water and porous layers, respectively, F_ε the boundary absorption term, F_B the wave breaking dissipation term, C_r the inertial coefficient, t the time and x the horizontal coordinate. Subscripts denote partial differentiation. α denotes the resistance coefficient of the porous medium:

$$\alpha \equiv \alpha_1 + \alpha_2 |u_s| = \frac{\nu\varepsilon}{K} + \frac{C_f \varepsilon^2}{\sqrt{K}} |u_s| \quad (4)$$

where ν is the kinematic viscosity, K the intrinsic permeability and C_f is the turbulent friction coefficient. φ and φ_s are the extended dispersion terms defined as

$$\varphi \equiv \left(\frac{1}{3} + \gamma \right) h^2 u_{xxt} + \left(\frac{1}{2} + \gamma \right) h h_x u_{xt} + \left(\frac{1}{2} + \gamma \right) h (h_x u_t)_x + \gamma g h (h \eta_x)_{xx} + \frac{1}{2} h (h_p u_{st})_{xx} \quad (5)$$

$$\begin{aligned} \varphi_s \equiv & \frac{1}{2} C_r \left[\frac{2}{3} h_s^2 u_{sxx} + h_s (h_{bx} u_{st})_x - h_s (h_x - h_{sx}) u_{sxt} - 2 h_x h_{bx} u_{st} \right] \\ & + \frac{1}{2} \alpha \left[\frac{2}{3} h_s^2 u_{sxx} + h_s (h_{bx} u_s)_x - h_s (h_x - h_{sx}) u_{sx} - 2 h_x h_{bx} u_s \right] + \frac{1}{2} (h^2 u_t)_{xx} \\ & + (1 + \beta) \left[h (h_p u_{st})_x \right]_x + \frac{\beta g}{C_r} \left[h (h_p \eta_x) \right]_x + \frac{\beta g}{C_r} \left[h (h_p u_s)_x \right]_x \end{aligned} \quad (6)$$

where $h_p \equiv \epsilon h_s$ is the effective porous thickness, $h_b \equiv h + h_s$ the bottom depth, and γ and β the celerity and damping extension factors. The right sides of **Eqs. (1) to (3)** indicate the truncation error in the dispersivity parameter $\mu \equiv h_o/l$ and nonlinearity parameter $\delta \equiv a/l$ where h_o , l and a are the characteristic depth, wavelength and amplitude, respectively.

Linear Analysis of Model Equations

A linear analysis of the model equations has been carried out by neglecting the dynamic volume flux term in Eq. (1), the convective terms in Eqs. (2) and (3) and the nonlinear resistance term α_2 in α . This leads to the following dispersion relation for porous beds:

$$\frac{\omega^2}{k^2 gh} \left[1 + \left(\frac{1}{3} + \gamma \right) k^2 h^2 \right] \left\{ \left(C_r + i \frac{\alpha}{\omega} \right) \left(1 + \frac{1}{3} k^2 h_s^2 \right) + k^2 h h_p \left(1 + \beta + i \frac{\beta \alpha}{\omega C_r} \right) \right\} = \left(1 + \gamma k^2 h^2 \right) + \frac{h_p}{M h} \left[1 + \left(\frac{1}{3} + \gamma \right) k^2 h^2 \right] \left[1 + \frac{\beta}{C_r} k^2 h h_p \right] \tag{7}$$

$$- \frac{k^2 h h_p}{2 M} \left[\left(1 + \frac{\beta}{C_r} k^2 h h_p \right) - \frac{\omega^2 h}{g} + \left(1 + \gamma k^2 h^2 \right) \right] M = \left(C_r + i \frac{\alpha}{\omega} \right) \left(1 + \frac{1}{3} k^2 h_s^2 \right) + \lambda k^2 h h_s \left(1 + \beta + i \frac{\beta \alpha}{\omega C_r} \right) \tag{8}$$

For progressive waves of angular frequency ω , the complex wave number k consists of a real part k_r that governs the phase celerity and an imaginary part k_i which gives the spatial porous damping rate. The values of γ and β have been determined by comparing these wave properties with those of the theoretical dispersion relation for porous beds up to deep water. Eq. (7) reduces to the dispersion relation of Madsen et al. (1991) when $h_p=0$. **Fig. 5(a)** plots the normalized celerity r_1 as a function of frequency in terms of h/L_0 , where $L_0=2\pi g/\omega^2$, for various relative porous thickness h_s/h . **Fig.5(b)** shows the dependence of the normalized damping rate r_2 on frequency. Plots similar to **Fig. 1** were obtained for values up to $\epsilon=0.7$.

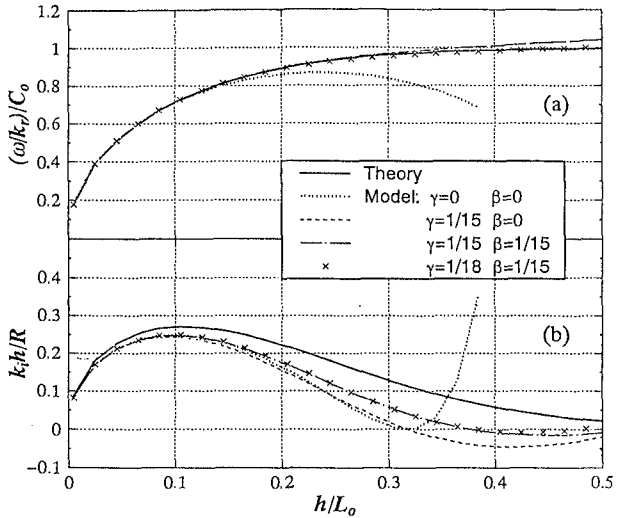


Fig.5 Summarized curve of r_1 (a) and r_2 (b) of the extended model equations

which leads to the optimum values $\gamma=1/21$ and $\beta=1/15$ up to $h/L_0=0.50$, $h_s/h=10$, $\varepsilon=0.7$ and $R=1.0$. These upper limits of the wave and porous layer parameters already encompass their practical limits.

Wave Breaking Dissipation

Due to the steep seaward slope, wave breaking occur mostly as plunging breakers. At present however, there is no adequate model for plunging random breakers even for solid beds. In this simplified treatment, a surface roller approach (Deigaard, 1989; Schaffer et. al., 1992) ignoring the effects of the porous bottom is employed.

$$F_B = \frac{\partial \psi}{\partial x} = \frac{\partial}{\partial x} \left[\frac{\delta(h + \eta - \delta)}{(h + \eta)^2} (C - u)^2 \right] \tag{9}$$

Where, ψ is momentum flux correction, δ the roller thickness, C the wave celerity. In this model, breaking is determined based on the crest toe angle. The roller approach is adopted due to its ability to deal with temporally and spatially migrating breakers as obtained in an irregular wave field on a non-monotonic bathymetry.

Velocity Field

The fluid particle horizontal velocities can be obtained from the depth-averaged velocities by invoking their definitions in terms of the velocity potentials. The horizontal velocity U in the water layer is given by

$$U(z) = u - \frac{1}{2} \left[(z+h)^2 - \frac{h^2}{3} \right] u_{xx} - \frac{1}{2} (h+2z) [(h_x u)_x + h_x u_x] - \frac{\varepsilon}{2} (h+2z) (h_s u_s)_{xx} \tag{10}$$

and the velocity U_s in the porous layer by

$$U_s(z) = u_s + \frac{1}{2} \left\{ \left(\frac{h_s^2}{3} + h h_b - z^2 \right) u_{sxx} + [h_s - 2(z+h_b)] (h_b u_s)_{xx} \right\} \tag{11}$$

where z is taken positive upward from the still-water level. Eqs. (10) and (11) satisfy the following boundary condition at the interface $z=-h(x)$,

$$U_n = \varepsilon U_{s,n} \tag{12}$$

where n denotes the direction normal to the interface. The velocity potential, when truncated at the order consistent with Eqs. (2) and (3), therefore, prescribes a parabolic vertical distribution of horizontal velocities in both layers.

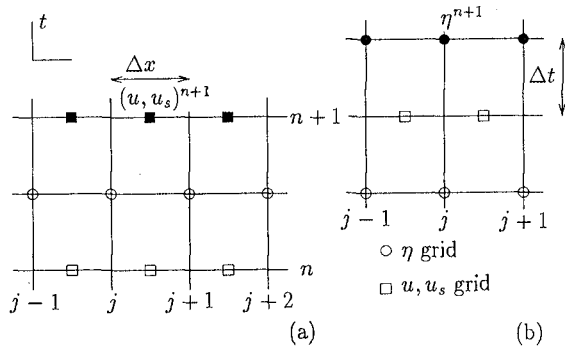


Fig.6 Finite difference module for solution of model equations.

4. NUMERICAL COMPUTATIONS

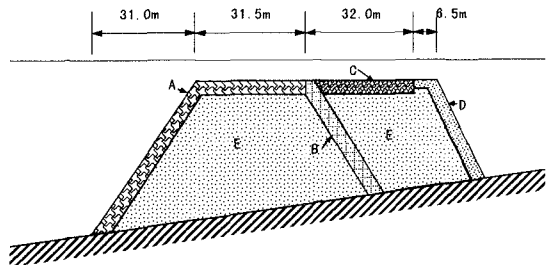
Eqs. (1) to (3) were discretized using the finite difference method on a staggered grid (Fig. 6). η is defined on the main grid, u and u_s on the secondary grid and the depths h, h_s on both grids. Eqs. (2) and (3) are first solved for u and u_s , and then Eq. (1) is used to solve for η in alternating time steps spaced at $\Delta t/2$.

Waves are introduced at the left end of the computation domain and the transmitted waves exit the open boundary at the right end. Because waves are reflected from the steep seaward slope of the reef, numerical wave absorbers were placed on both ends to absorb the outgoing wave components. The properties of the absorber, namely, its damping distribution, maximum damping coefficient and absorber width were determined from simulation aid graphs theoretically developed for regular and irregular wave fields (Cruz and Isobe, 1994). Computations were continued until the wave profile has become stable from one period to the next. Considering the presence of absorbers at both ends, this condition is achieved after the first crest has traveled a distance of about $5X_D$, where X_D is the total width of the computation domain.

Reef Material Distribution

The vertical section at the centerline of the reef, Fig. 1(b), was taken as the representative section for the preliminary one-dimensional calculation reported here. Due to the variability of materials in the reef armor and interior, reef porosity is not uniform. Fig. 7 shows the cross-section make-up of the present Yugawara Reef along its centerline. The previous 32-meter reef was formed with medium-sized rocks and covered with 10ton X-blocks. The added portion has an interior similar to the older one but was protected with different armors. To carry out wave simulations, however, it was necessary to use a uniform porosity in the model equations. Noting that the flow field near the seaward corner of the crown is critical, we used values of the material properties based on the X blocks and assumed that the entire reef is a homogeneous structure. For purposes of analysis, it was assumed to be uniform. In the simulation, The following parameters were used:

$$\begin{aligned} \epsilon &= 0.20, \nu = 1.3 \times 10^{-6} \text{ m}^2/\text{s} (10^\circ \text{C}), \\ K &= 8 \times 10^{-7} \text{ m}^2, C_f = 0.20 \end{aligned}$$



Zone	Material	Weight
A	X-Blocks	10tons
B	armor rocks	250kg
C	armor rocks	2tons
D	armor rocks	500~800kg
E	medium-size rocks	30~200kg

Fig.7 Reef material distribution of Yugawara artificial reef.

K and C_f were obtained by linearly extrapolating the data of Sollit and Cross (1972) for a mean block size of 1.0m.

Simulation of the Regular Wave Field (Non-breaking)

To examine the characteristic of the model, simulation is performed using regular waves. In order to utilize the field data, the incident wave has the properties of the significant wave, namely, $T_{in} = (T_{1/3})_{Sta.0}$ and $H_{in} = (H_{1/3})_{Sta.0}$. The spatial profiles of η at $T_{in}/8$ intervals beginning at $t=t_{rec}$ are shown in Fig. 8(a). The incident wave is linear at station 0 (Ursell No. $Ur=0.17$) and becomes

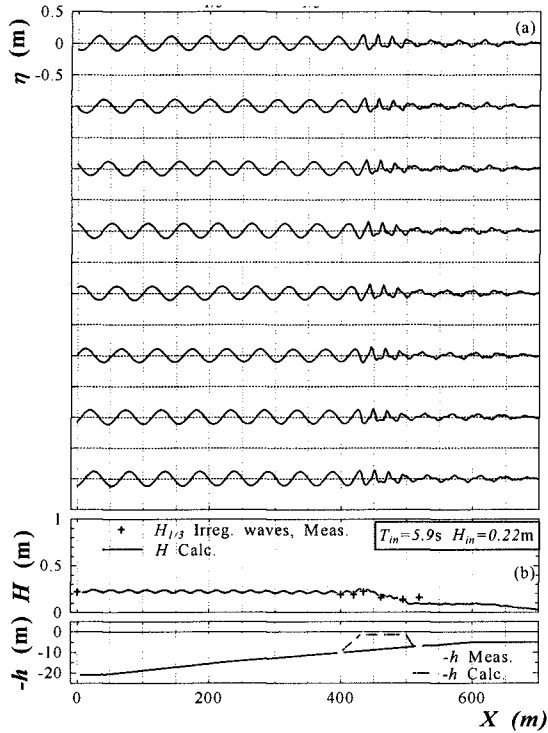


Fig. 8 Wave field (a) Simulated evolution of η (b) Comparison of calculated and measured

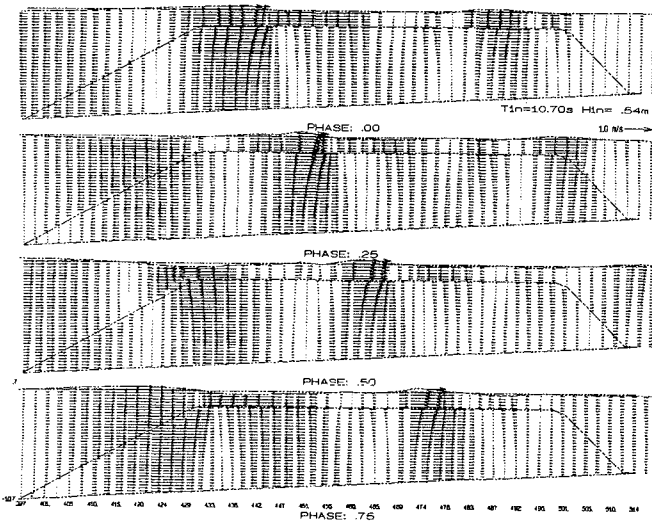


Fig. 9 Vertical field of U and U_s at $T_{in}/4$ intervals

nonlinear at the reef crown because of its shallowness. Higher harmonics are generated on the crown and the resultant wave propagates largely undeformed on the crown (ignoring the damping effect of the reef) because the higher harmonics and the primary wave travel at essentially at the shallow-water celerity. These bound harmonics are released behind the reef as free-waves that travel at their frequency-dependent celerities. Further leeward, the free waves interact with each other and the primary wave resulting in the nonpermanent profiles as seen in the figures.

Fig. 8(b) show the comparison of the simulated wave heights H and the significant wave heights $H_{1/3}$ of the field data. Prior to the crown, these wave heights agree very well. The underestimation of H at station 6 is partly due to the neglect of reflection from the revetment which has been confirmed in the field measurements (Ohnaka and Yoshizawa, 1994).

The spatial distribution of the velocities can be used to obtain the vertical field of fluid particle velocities U and U_s through Eqs. (10) and (11). **Fig. 9** show the velocity profile at the reef toe is that of linear wave. As the wave moves into the crown, the upper portion of the reef is engaged in redistributing the wave energy through the interface boundary conditions, for example, Eq. (11). The wave crest does not have to travel far into the crown because a relatively thick porous medium is available to dissipate a relatively small interface velocity.

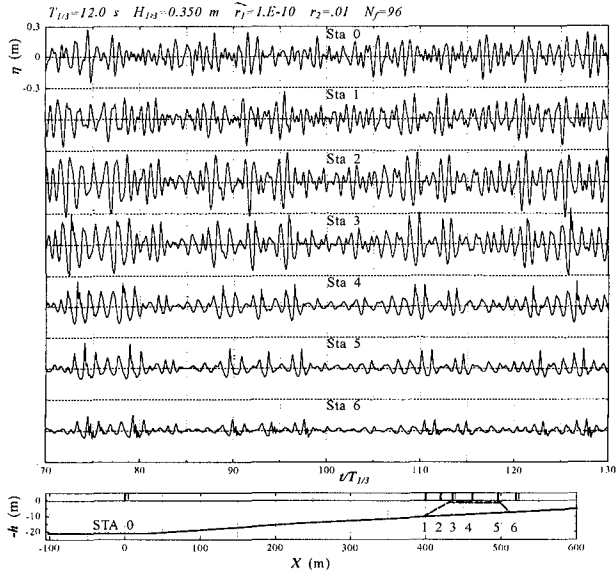


Fig. 10 Simulated evolution of η

Simulation of Irregular Wave Field Non-Breaking Wave

Fig. 10 shows the results of the simulation of an irregular non-breaking

wave. The input frequency spectrum is Bretschneider-Mitsuyasu type with a period of 12.0 s and height of 0.35m. The time profile at Station 0 is generated using linear random wave theory consisting of 256 waves with random phases. Simulations are done for 138 significant periods and the last 128 periods

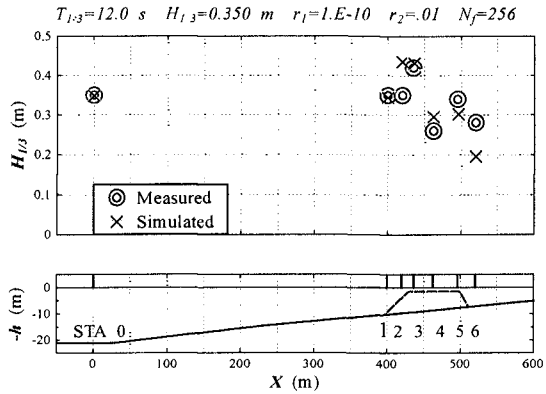


Fig. 11 Comparison of calculated and measured wave heights are used for synthesis.

In Fig. 10, the time profiles at Stations 0 to 6 for the last 60 periods is shown. In particular, the frequency components are reduced drastically by passage on the reef. At the back, the high-frequency portion is somewhat recovered. Fig. 11 shows the measured and simulated significant wave heights. Dominant shoaling effect at Station 1 is simulated well and the high wave on Station 3 is satisfactorily predicted. However, deviations are noticeable for the shoreward Stations.

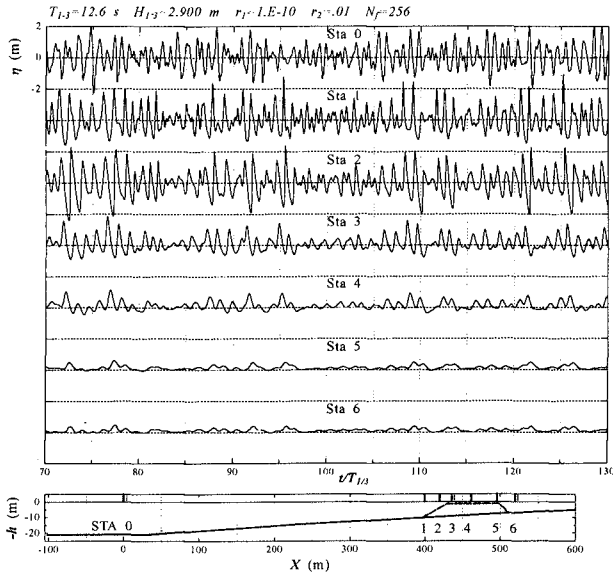


Fig. 12 Simulated evolution of η (breaking wave)

Breaking Wave

Fig. 12 shows the time profiles for the simulation of the highest recorded significant wave at Station 0 with incident wave height of 2.90 m and period of 12.6 s. Compared to the nonbreaking case, high-frequency reduction of the incident profile

occurs earlier. This is attributed to the active damping by the porous layer when the velocity penetrates the reef interior. However, breaking between Stations 2 and 3 still causes the major reduction in wave energy. **Fig. 13** shows the significant wave heights. The high wave on the slope is still predicted well but there is considerable underestimation of wave energy beginning at Station 3. The trend of wave height is still predicted correctly.

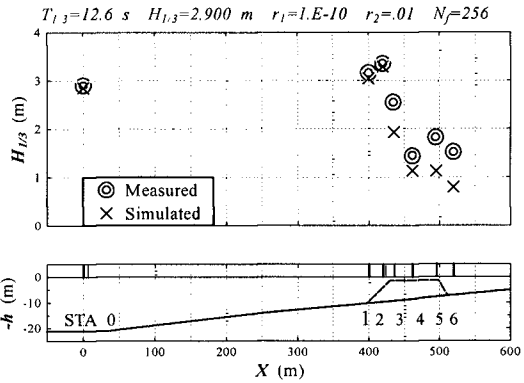
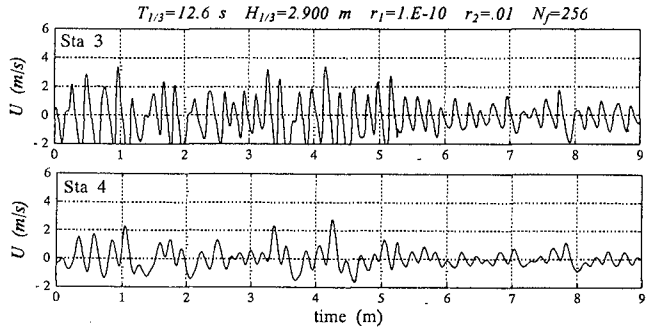


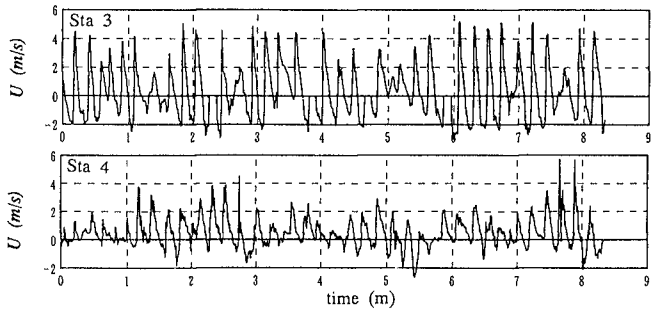
Fig. 13 Comparison of calculated and measured wave height (breaking wave)

Simulation of the Velocity Field

The velocity field is obtained simultaneously in the solution of Eqs. (1) to (3). **Fig. 14** shows the time series of depth-averaged horizontal velocity in water layer at Stations 3 and 4 on the reef crown for the breaking wave case. Since the crown is shallow at these stations, the measured point velocity essentially represents the depth-averaged value. Segments of the velocity measured at the current meters located 70 cm above the crown are shown for comparison. Although a direct comparison of the ob-



(a) calculated velocity



(b) observed velocity

Fig. 14 Time series of the calculated and measured velocity *u*.

served and simulated velocities is strictly not meaningful due to the different phase relationships in the incident wave, the profiles indicate the velocity magnitudes after breaking. The simulation based on a depth-averaged treatment of the momentum exchange in a breaker tends to overestimate the amount of energy dissipated on the crown primarily because the breaking point predicted by the model occurs seaward of the reef crown, resulting in a wider region within which energy is apparently decimated. A surface roller approach tends to be sensitive to reflection which leads to a preemptive prediction of breaking.

Fig.15 shows the root-mean-square depth-averaged velocities u_{rms} obtained by a second run in which the roller parameters were determined such that the breaking point occurs just before the reef crown. In this case, u_{rms} are closer to the measured values especially before the breaking point and the general trend is predicted well. However, the values are significantly underestimated beyond Station 3 due to various factors, the most important of which is the variable material makeup of the actual reef.

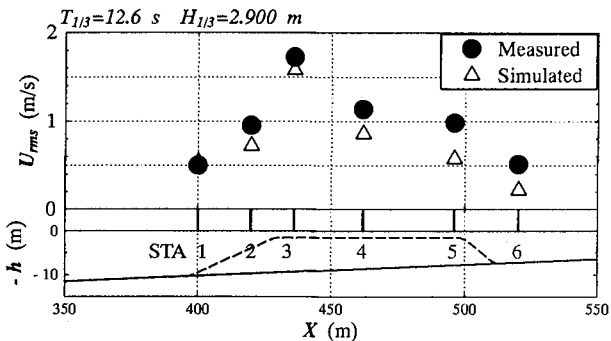


Fig. 15 Comparison of calculated and measured rms value of velocities.

5. CONCLUSIONS

The following summarizes the leading conclusions of this study:

- a. Measurements of the wave and current fields around the existing Yugawara Reef in Japan are reported. A synthesis of the significant wave parameters is discussed.
- b. A set of nonlinear wave equations with an extended range of dispersivity and porous damping rate is used to simulate the nonbreaking wave field along the reef centerline. Breaking waves are modelled using surface rollers.
- e. The wave field is generally characterized by a strong seaward reflection, decaying

wave heights on the crown and decomposing waves beyond the reef.

- d. There is a general agreement of wave energy distribution around the reef. However, deviations from measured values are observed. These are attributed to the simplifications in modelling the material composition of the reef, directional nature of the incident wave spectrum, the assumed two-dimensionality of the wave field and boundary influences such as external reflections.

Reference

- Cruz, E.C., M. Isobe and A. Watanabe (1992): Nonlinear wave transformation over a submerged permeable breakwater. Proc., Int. Conf. Coastal Eng., pp.1101..1114.
- Cruz, E.C., M. Isobe and A. Watanabe (1996): Boussinesq equations for wave transformation on porous beds, Coastal Eng., CENG 00727.
- Cruz, E.C. and M. Isobe (1994): Numerical wave absorbers for short and long wave modelling. Proc., Int. Symp. on Waves -- Phys. and Num. Modelling. Univ. of British Columbia, pp.992..1001.
- Deigaard, R.(1989): Mathematical modelling of waves in the surf zone, Progress Rep. 69, ISVA, Tech. Univ., Lyngby, Denmark, pp.47-59.
- Hasimoto, N., T. Nagai and T. Asai (1994):Extension of the maximum entropy principle method for directional wave spectrum estimation, Proc., Int. Conf. Coastal Eng., pp.232..246.
- Isobe, M., K. Shiba, E.C. Cruz and A. Watanabe (1991): On the nonlinear deformation of waves over submerged permeable breakwaters. Proc., Coastal Eng. Conference in Japan (in Japanese). pp.551..555.
- Ohnaka, S. and T. Yoshizawa (1994): Field observation on wave dissipation and reflection by an artificial reef with varying crown width. Proc., Int. Conf. Hydro-Technical Eng. for Port and Harbor Construction, pp.365..376.
- Madsen, P.A., R. Murray and O.R. Sorensen (1991): A new form of the Boussinesq equations with improved linear dispersion characteristics. Coastal Eng., 15, pp. 371..388.
- Schaffer, H.A., R. Deigaard and P.A. Madsen(1984): A two dimensional surf zone model based on the Boussinesq equations, Proc., Int. Conf. Coastal Eng., pp.576-589.